

Absorbing-state transitions in particulate systems under spatially varying driving

Bhanu Prasad Bhowmik* and Christopher Ness

School of Engineering, University of Edinburgh, Edinburgh EH9 3JL, United Kingdom

We study the absorbing state transition in particulate systems under spatially inhomogeneous driving using a modified random organization model. For smoothly varying driving the steady state results map onto the homogeneous absorbing state phase diagram, with the position of the boundary between absorbing and diffusive states being insensitive to the driving wavelength. Here the phenomenology is well-described by a one-dimensional continuum model that we pose. For discontinuously varying driving the position of the absorbing phase boundary and the exponent characterising the fraction of active particles are altered relative to the homogeneous case.

Introduction. The response of soft materials to cyclic deformation is a subject of intense research due to its relevance to liquefaction [1], hopper unblocking [2] and yielding [3]. This process gives rise to phenomena of fundamental interest, including absorbing state transitions and self-organized criticality [4–8], mechanical annealing [9] and fatigue failure [10]. Most work to date focuses on homogeneous cases in which the externally applied driving shear rate is spatially uniform, though in practical scenarios the driving is almost certain to be inhomogeneous. Recent studies in various soft materials [11–15] reveal that the rheology of systems under homogeneous and inhomogeneous driving often differs qualitatively, so that the response to the latter cannot necessarily be fully predicted based on the former.

Here we focus on the non-equilibrium absorbing state transition in athermal particulate systems below jamming. Under cyclic deformation with driving amplitude γ less than a volume (or area) fraction ϕ dependent threshold $\gamma_c(\phi)$, such systems attain special configurations which reappear precisely after full cycles of deformation, so that, when viewed stroboscopically (with a period of 1 or occasionally more cycles [16]), the system does not explore configuration space. Above γ_c there exist active particles (C_A) that do not return to their initial positions so that the self-diffusion coefficient is nonzero. These states are separated by a critical line on the $\phi - \gamma$ phase diagram, exhibiting an equilibrium-like continuous transition with C_A serving as the order parameter.

To study the physics of this transition it has proven useful to explore ‘random organization’ models [5, 17–20], whose predictions suggest it belongs to the conserved directed percolation (CDP) class, though this is altered in the presence of multiple or mediated interactions [21, 22]. Thus far, such models are reported for homogeneous driving only, yet in practical scenarios involving cyclic driving of particulates the driving rate may inherently be non-uniform. More broadly the role of spatial inhomogeneity in processes with absorbing states is relevant to regionally varying immunity levels in disease spreading scenarios, or to reaction-diffusion problems with spatially varying catalytic activity. In order to gain fundamental insight into this more complex class of problems it is thus crucial to

determine whether the presence of spatially varying driving forces affects the nature and position of absorbing state transitions in discrete systems, and, importantly, whether homogeneous measurements predict the properties of inhomogeneous systems.

We use a modified isotropic random organization model [17, 23] to study the absorbing state transition under inhomogeneous driving. The control parameters are the overall area fraction $\bar{\phi}$ of particles of diameter σ and their per-step displacement Δ . The latter is an analogue of the oscillatory strain amplitude γ , and we impose spatial dependence $\Delta(y)$ to represent *e.g.* the spatially-varying strain rate present in a flowing system. For diffusive states we observe in the results a spatial inhomogeneity with the local area fraction at y , $\phi(y)$, being lower in regions where the driving amplitude $\Delta(y)$ is large. For smoothly varying driving ($\partial\Delta/\partial y$ exists at every point) with wavelength $L_y/\sigma = 7.7 - 400$, the local active particle concentration $C_A(y)$ matches that obtained under homogeneous conditions at the same $\Delta(y)$ and $\phi(y)$, indicating that the presence of gradients does not influence the properties of the $\Delta - \phi$ phase diagram. We thus explore a continuum model modified to account for inhomogeneous driving, and find it supports our simulation results, albeit with the expected mean-field exponents [24, 25]. Conversely, for discontinuous $\Delta(y)$ inhomogeneous effects play a role and the properties of the phase diagram depend on the length L_c over which the driving remains uniform. For $L_c/\sigma \lesssim 20$, the position of the absorbing boundary depends on L_c , while for the extreme case in which $\Delta = 0$ for a small fraction of particles C_p , the position and exponent of the transition are C_p -dependent, indicating a change to the universality class.

Simulation details. We simulate $N = 5000 - 30000$ disks with diameter chosen from a Gaussian with mean σ and standard deviation 0.2σ in a box of area $L_x \times L$ (with L an integer multiple of L_y , defined below). Initially random configurations having widespread particle overlaps evolve according to the following deterministic rules. Particles not overlapping with any other are inactive and do not move. Particles with $Z > 0$ overlapping neighbors are active and their positions \mathbf{r}_i are updated following $\mathbf{r}_i(t + \delta t) = \mathbf{r}_i(t) + \Delta_i \delta t \sum_{j=1}^Z \mathbf{n}_{ij}$, where \mathbf{n}_{ij}

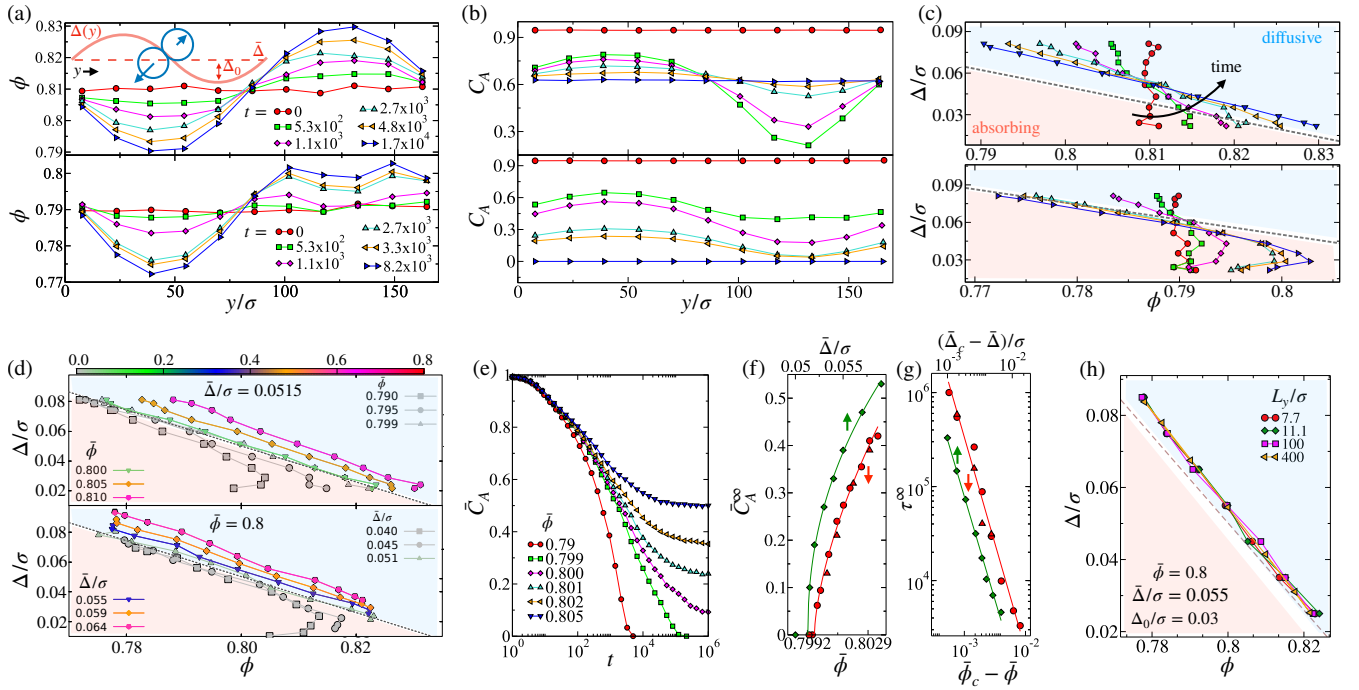


FIG. 1. Absorbing-state transition in inhomogeneously driven particulate material. Shown are the time evolution of (a) area fraction $\phi(y)$ and (b) active particle concentration $C_A(y)$, for systems with steady states lying above (top, $\bar{\phi} = 0.81$) and below (bottom, $\bar{\phi} = 0.79$) the absorbing phase boundary, with $\bar{\Delta}/\sigma = 0.0515$, $\Delta_0/\sigma = 0.03$ and $L_y/\sigma = 160$. The Inset of (a) is a schematic of the dynamics; (c) The $\Delta - \phi$ phase space showing parametrically $\phi(y)$ and $\Delta(y)$ at progressing time. The dashed line represents the homogeneous phase boundary separating absorbing (pink) and diffusive (blue) states (legend in (a) applies also to (b) and (c)); (d) Steady state $\Delta - \phi$ lines for $\bar{\Delta} = 0.0515$ at a range of $\bar{\phi}$ (top) and $\bar{\phi} = 0.8$ at a range of $\bar{\Delta}$ (bottom), with $\Delta_0 = 0.03$. Colorbar represents the magnitude of $C_A(y)$ (which is approximately uniform in space); (e) Time evolution of mean active particle concentration \bar{C}_A for various $\bar{\phi}$ keeping $\bar{\Delta}$, Δ_0 fixed; (f) Variation of \bar{C}_A^∞ with $\bar{\phi}$ at fixed $\bar{\Delta}$ (red) and $\bar{\Delta}$ at fixed $\bar{\phi}$ (green (circles are $L_y/\sigma = 120$; triangles are $L_y/\sigma = 11$)); (g) Variation of the time τ^∞ required to reach absorbing states when below the phase boundary, with $\bar{\phi}$ (green) and $\bar{\Delta}$ (red). Solid lines in (f) and (g) are fits to $f(x) = f_0(x - x_c)^a$. (h) Example steady state $\Delta - \phi$ lines (parameters in legend) showing independence of L_y in the diffusive regime.

are unit vectors pointing from particle i to each of its contacts j , Δ_i is the kick size for the i^{th} particle, and $\delta t = 1$. The overall area fraction is $\bar{\phi} = \frac{\sum_{i=0}^N \pi \sigma_i^2}{4L_x L}$. We produced the $\Delta - \phi$ phase diagram for spatially-invariant Δ (finding results consistent with [17, 26]) and refer to it in what follows. For inhomogeneous driving we initially let Δ_i be smoothly varying as $\Delta_i(y_i) = \bar{\Delta} + \Delta_0 \sin(\frac{2\pi y_i}{L_y})$, Fig. 1(a) [Inset]. The inputs to our model are thus $\bar{\phi}$, $\bar{\Delta}$, Δ_0 and L_y , while the observables we compute are the spatial profiles of the area fraction $\phi(y) = \frac{1}{L_x} \int_0^{L_x} \phi(x, y) dx$ and the active particle concentration $C_A(y) = N_A(y)/N(y)$, with $N_A(y)$ and $N(y)$ the number of active and total number of particles at position y . Coarse grained profiles are computed by binning particles in y before averaging the particle properties in each bin. Results are averaged across 50 realisations for each parameter set. We define the order parameter $\bar{C}_A = \frac{1}{L} \int_0^L C_A(y) dy$, and \bar{C}_A^∞ as its steady state value.

Smoothly varying $\Delta(y)$. Using sinusoidal $\Delta(y)$ we explore a range of $\bar{\Delta}$ (letting $\Delta_0 = 0.03\sigma$), $\bar{\phi}$ and L_y , to investigate conditions that in principle span across the

homogeneous absorbing state phase boundary. Model predictions are shown in Fig. 1. Inhomogeneous driving produces steady states with spatially varying ϕ , with regions of higher $\Delta(y)$ having lower $\phi(y)$, Fig. 1(a), in agreement with experiment [27, 28] and simulations with more detailed physics [11, 12, 29]. The local active particle concentration $C_A(y)$ varies in the opposite direction to $\phi(y)$ at small t , before reaching steady states that are spatially uniform, Fig. 1(b). For $(\bar{\phi}, \bar{\Delta})$ above the homogeneous phase boundary (top panels of (a),(b)), the inhomogeneous system remains diffusive at long times with $C_A(y) > 0$, whereas below the homogeneous phase boundary $C_A(y) = 0$ everywhere in the system. The system never produces mixed absorbing-diffusive steady states with $C_A(y)$ only locally vanishing.

Each inhomogeneous simulation produces a set of parametric points corresponding to lines across the $\Delta - \phi$ phase diagram, bounded by $\Delta = \bar{\Delta} \pm \Delta_0$, Fig. 1(c). Initial configurations with uniform $\phi(y)$ appear as vertical $\Delta - \phi$ lines, before evolving with time. Since the local activity at y is controlled by both $\phi(y)$ and $\Delta(y)$, particles in regions with higher Δ will have higher mobility and

move to regions with lower Δ , resulting in an increment of the area fraction in those regions. This consequently increases the activity of those regions. Thus, regions with initial local parameters below the absorbing phase boundary can increase in $\phi(y)$ and thus become active. This process manifests as a counterclockwise rotation of $\Delta - \phi$, Fig. 1(c) (top). For $(\bar{\phi}, \bar{\Delta})$ above the homogeneous phase boundary, after this transient the system attains a diffuse steady state with $\Delta(y)$ and $\phi(y)$ balanced such that $C_A(y)$ becomes spatially uniform. For $(\bar{\phi}, \bar{\Delta})$ below the phase boundary, the large- Δ regions do not inject enough particles to the small- Δ regions to trigger activity, thus leaving those areas with the same conditions as at the beginning of the simulation and the resultant hook shape in Fig. 1(c) (bottom).

Figure 1(d) shows steady state $\Delta - \phi$ lines as functions of $\bar{\phi}$ (top) and $\bar{\Delta}$ (bottom). The colorbar stands for the magnitude of $C_A(y)$, which decreases as $(\bar{\phi}, \bar{\Delta})$ approaches the phase boundary from within the diffusive phase, and vanishes in the absorbing state. Interestingly, the location of the critical line at which $C_A(y)$ vanishes overlaps with the homogeneous absorbing phase boundary (dashed lines, Fig. 1(d)), so that in principle a single inhomogeneous simulation can identify the entire homogeneous phase boundary. In Fig. 1(e) the variation of \bar{C}_A with time is shown for various $\bar{\phi}$ at fixed $\bar{\Delta}$, Δ_0 . As in the homogeneous case, \bar{C}_A vanishes at low $\bar{\phi}$, indicating that absorbing states exist, whereas above it saturates to non-zero steady states \bar{C}_A^∞ which we characterise by fitting the data to $C_A(t) = c_0 e^{-(t/t_0)^{c_1}} + \bar{C}_A^\infty$, where c_0 , t_0 and c_1 are fitting parameters.

As \bar{C}_A^∞ serves as our order parameter, we investigate the details of the absorbing state transition by examining its dependence on the parameters. The measured values follow $\bar{C}_A^\infty \sim (\bar{\phi} - \bar{\phi}_c)^{\beta_\phi}$ for fixed $\bar{\Delta}$ and $\bar{C}_A^\infty \sim (\bar{\Delta} - \bar{\Delta}_c)^{\beta_\Delta}$ for fixed $\bar{\phi}$, Fig. 1(f), and we find $\beta_\phi = 0.64$, in agreement with Refs [18, 24], $\bar{\phi}_c = 0.7996$, and $\beta_\Delta = 0.45$, close to the values reported by Ref [5], with $\bar{\Delta}_c = 0.0513$. Additionally, as the system approaches the critical line from the absorbing phase, the time required to reach steady state diverges as $\tau^\infty \sim (\bar{\phi} - \bar{\phi}_c)^{\nu_\phi}$ for fixed $\bar{\Delta}$ and $\tau^\infty \sim (\bar{\Delta} - \bar{\Delta}_c)^{\nu_\Delta}$ for fixed $\bar{\phi}$, Fig. 1(g). We find $\nu_\phi = 1.37$ with $\bar{\phi}_c = 0.7994$, and $\nu_\Delta = 1.33$ with $\bar{\Delta}_c = 0.0513$, in close agreement with previous studies [5, 18, 24]. Thus the position and nature of the phase boundary obtained under inhomogeneous conditions matches the homogeneous case. We verified that this holds for $L_y/\sigma = 7.7 - 400$, Figs. 1(f)-(h).

Continuum model. Given that the phase boundary is governed by local conditions only, we introduce a continuum model (Manna class [30, 31] without noise [32]) modified for inhomogeneous driving by introducing convection in the system. Herein $\phi_A(y, t)$ and $\phi_I(y, t)$ are the area fraction of active and inactive particles, related through $\phi(y, t) = \phi_A(y, t) + \phi_I(y, t)$, $\dot{\phi} = \dot{\phi}_A + \dot{\phi}_I$, and

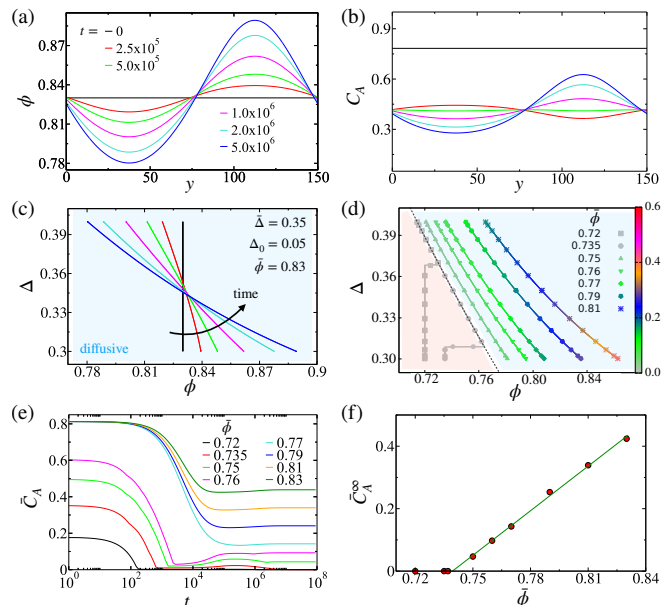


FIG. 2. Predictions of continuum model. Shown are the time evolution of (a) $\phi(y)$, (b) $C_A(y)$ and (c) the $\Delta - \phi$ line, from initialization up to a steady state in the diffusive regime (parameters in Legend of (c)). The color scale in (a) applies also to (b) and (c); (d) Steady state $\Delta - \phi$ lines for various $\bar{\phi}$ at fixed profiles of $\Delta(y)$; colorbar shows the magnitude of $C_A(y)$. (e) Time evolution of \bar{C}_A for a range of $\bar{\phi}$ spanning the absorbing phase boundary; (f) Variation of $\bar{C}_A^\infty(y)$ with $\bar{\phi}$ keeping the $\Delta(y)$ profile fixed, with solid line as in Fig. 1(f).

with $C_A = \phi_A/\phi$. The dynamics are given by

$$\begin{aligned} \dot{\phi}_A &= \nabla(\mathcal{D}\nabla\phi_A) + \nabla(\nabla\Delta\phi_A) \\ &\quad + \alpha\phi_A(\phi - \phi_A) - \beta\phi_A(1 - \phi), \end{aligned} \quad (1)$$

$$\dot{\phi}_I = -\alpha\phi_A(\phi - \phi_A) + \beta\phi_A(1 - \phi), \quad (2)$$

where $\nabla = \frac{\partial}{\partial y}$, and α and β are positive coefficients. α represents activation of particles by interaction with active neighbours; β represents isolated death (we omit caging [33]). The convection term in Eq. 1 arises due to spatially-varying driving. The diffusion coefficient is taken as $\mathcal{D}(y) \sim \Delta^2(y)/\tau$, with the time scale τ taken as unity. The phase boundary can be estimated from the condition $\phi_A = 0$, $\nabla\phi_A = 0$ and $\dot{\phi}_A = 0$. The coefficient α is directly related to Δ , and for simplicity we choose $\alpha \sim \Delta$. Thus the critical mean kick size $\bar{\Delta}_c$ representing the phase boundary at a fixed $\bar{\phi}$ is $\bar{\Delta}_c = \beta/\bar{\phi} - \beta$. We solve these coupled equations numerically, with $\Delta(y) = \bar{\Delta} + \Delta_0 \sin(\frac{2\pi y}{L_y})$ and initial conditions $\phi(y) = \bar{\phi} = 0.83$, $\phi_A(y) = \phi_A^0 = 0.65$ using $\bar{\Delta} = 0.35$, $\Delta_0 = 0.05$. Shown in Figs. 2(a)-(c) are transients of $\phi(y)$ and $C_A(y)$ in the diffusive regime, showing qualitative agreement with Figs. 1(a)-(c) (top). In Fig. 2(d) are steady state $\Delta - \phi$ lines spanning the absorbing phase boundary, qualitatively matching the random organization model predictions in Fig. 1(d). In the absorbing

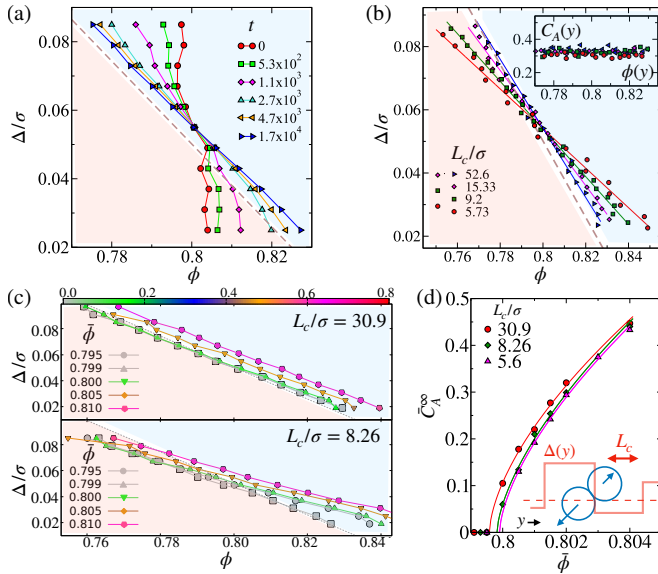


FIG. 3. Model predictions with discontinuous $\Delta(y)$. (a) Time evolution of $\Delta - \phi$ for $\bar{\phi} = 0.80$, with $\bar{\Delta} = 0.056$, $\Delta_0 = 0.03$ and $L_c/\sigma = 52.6$, showing similar behaviour to the smoothly varying case; (b) Steady state $\Delta - \phi$ lines for $\bar{\phi} = 0.80$, $\bar{\Delta} = 0.054$ and $\Delta_0 = 0.03$, as a function of cell size L_c . Dashed line shows homogeneous absorbing state phase boundary. Inset: steady state $C_A(y)$ as a function of $\phi(y)$ for each case verifying that they are all diffusive despite crossing the boundary; (c) Steady state $\Delta - \phi$ lines for $\bar{\Delta} = 0.0515$, $\Delta_0 = 0.03$ at different $\bar{\phi}$ for $L_c = 30.9$ (top) and $L_c = 8.26$ (bottom). Grey dotted lines are the homogeneous absorbing phase boundary and the colorbar represents $C_A(y)$; (d) Variation of \bar{C}_A^∞ with $\bar{\phi}$, keeping $\bar{\Delta} = 0.0515$, showing the changing position of the boundary with L_c . Solid lines follow the form in Fig. 1(f). Inset: schematic of model dynamics.

state (gray lines) the hook shape in $\Delta - \phi$ appears as in the simulation, though with a sharper curve and a vertical profile at lower Δ where the dynamics cease quickly. The evolution of \bar{C}_A with time is shown in Fig. 2(e), approaching 0 and finite values respectively below and above the phase boundary with the time scale τ diverging at the transition. We find $\bar{C}_A^\infty \sim (\bar{\phi} - \bar{\phi}_c)^{\beta_c}$, with $\beta_c = 1$ agreeing with previously reported results [25, 33].

Discontinuous $\Delta(y)$. We next scrutinize the random organization model under discontinuously varying $\Delta(y)$. To do so we divide the system into cells of area L_c^2 , each having $\Delta = \bar{\Delta} + \Delta_r$ (Fig. 3(d) [Inset]), with Δ_r a random number chosen uniformly in the range $\pm\Delta_0$, ensuring $\sum_{i=1}^{N_c} \Delta_r = 0$, where N_c is the number of cells. Model predictions are shown in Fig. 3.

The transients observed for exemplar model parameters match qualitatively those from the smoothly varying model, Fig. 3(a), while steady state $\Delta - \phi$ data deviate significantly from the homogeneous absorbing state phase boundary, Fig. 3(b). As in the smoothly-varying scenario the active particles are distributed uniformly over the system in the diffusive regime, Fig. 3(b) [Inset]. For small

L_c , states that would be deep within the absorbing state remain active. This indicates that under discontinuously varying driving the absence or presence of an absorbing state cannot be determined using local knowledge of $\phi(y)$ and $\Delta(y)$: the size of the containing cell matters. Presumably particles near cell edges experience dynamics not described by Eqs. 1-2 due to proximal discontinuities in Δ . Indeed as L_c increases (and fewer particles are near cell edges), the data tend towards a diffusive line parallel to the homogeneous phase boundary as would be expected for locally-governed dynamics. In Fig. 3(c) steady state $\Delta - \phi$ lines are shown for $\bar{\Delta} = 0.0515$, $\Delta_0 = 0.03$ and a set of $\bar{\phi}$ crossing the homogeneous phase boundary (gray dotted line), for $L_c/\sigma = 30.9$ (top) and $L_c/\sigma = 8.26$ (bottom). The overall trend is similar to smoothly varying $\Delta(y)$, but importantly the position of absorbing phase boundary under randomly varying Δ does not match the homogeneous case, especially at small L_c (and indeed the large L_c and L_y cases do not appear to converge). Figure 3(d) shows the variation of \bar{C}_A^∞ with $\bar{\phi}$ at fixed $\bar{\Delta}$ for a range of L_c . The exponents match those in Fig. 1(f), but crucially but there is dependence of the critical point $\bar{\phi}_c$ on L_c .

We finally test the model for an extreme case of inhomogeneity in which a small subset of particles are permanently inactive. To do so we modify the above model by enforcing $\Delta = 0$ for a small fraction C_p of particles, chosen randomly. The remaining particles are assigned a fixed Δ , so that the mean kick size is now given by $\bar{\Delta} = (1 - C_p)\Delta$. Particles with $\Delta = 0$ remain frozen in their initial positions, equivalent to a pinning effect used widely in fundamental studies of various systems [34–36]. We run these dynamics for a range of C_p and $\bar{\phi}$, with $\Delta = 0.0515$. Shown in Fig. 4(a) is the resultant variation of the steady state \bar{C}_A^∞ . The points are simulation data, and solid lines are fits to $\bar{C}_A^\infty \sim (\bar{\phi} - \bar{\phi}_c)^\beta$. The critical area fraction $\bar{\phi}_c$ and exponent β both decrease with increasing C_p , Fig. 4(b)-(c), suggesting a change in the nature of criticality due to particle pinning [37].

Conclusions. We study the absorbing state transition in particulate systems under inhomogeneous driving us-

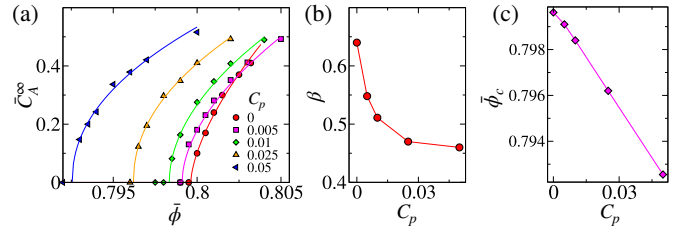


FIG. 4. Absorbing state transition with permanently inactive particle fraction C_p . (a) Steady state mean active particle concentration \bar{C}_A^∞ as a function of $\bar{\phi}$ for varying C_p with $\Delta = 0.0515$; Variation with C_p of (b) the critical exponent β and (c) the critical area fraction $\bar{\phi}_c$.

ing a modified random organization model. The resulting spatial variation in area fraction means each simulation produces a set of points in the $\Delta - \phi$ phase diagram, which are, in steady states, either entirely below or above the absorbing phase boundary. This behavior is reproduced with a simple continuum description of the system incorporating a convective term to account for spatially varying driving. When the driving varies smoothly in space the critical line separating absorbing from diffusive states is the same as for the homogeneous random organization model. Meanwhile for discontinuously varying driving the position of the absorbing phase boundary and its properties can deviate from the homogeneous case, suggesting that one might tune the position of an absorbing state boundary by manipulating the heterogeneity of the (discontinuous) driving. Our results show that the absorbing state boundary obtained under spatially homogeneous conditions can be used to predict the features of inhomogeneous systems only when the latter involves smoothly varying driving. Understanding the rich physics of absorbing states in particulate systems with discontinuously varying driving is thus a promising avenue of future fundamental research.

B.P.B. acknowledges support from the Leverhulme Trust under Research Project Grant RPG-2022-095; C.N. acknowledges support from the Royal Academy of Engineering under the Research Fellowship scheme.

* bhowmikbhanuprasad592@gmail.com

- [1] Y. Huang and M. Yu, *Natural hazards* **65**, 2375 (2013).
- [2] A. Janda, D. Maza, A. Garcimartín, E. Kolb, J. Lanuza, and E. Clément, *Europhysics Letters* **87**, 24002 (2009).
- [3] D. Bonn, M. M. Denn, L. Berthier, T. Divoux, and S. Manneville, *Reviews of Modern Physics* **89**, 035005 (2017).
- [4] D. J. Pine, J. P. Gollub, J. F. Brady, and A. M. Leshansky, *Nature* **438**, 997 (2005).
- [5] L. Corté, P. M. Chaikin, J. P. Gollub, and D. J. Pine, *Nature Physics* **4**, 420 (2008).
- [6] L. Corté, S. J. Gerbode, W. Man, and D. J. Pine, *Physical Review Letters* **103**, 248301 (2009).
- [7] K. Hima Nagamanasa, S. Gokhale, A. K. Sood, and R. Ganapathy, *Physical Review E* **89**, 062308 (2014).
- [8] D. Fiocco, G. Foffi, and S. Sastry, *Physical Review E* **88**, 020301 (2013).
- [9] H. Bhaumik, G. Foffi, and S. Sastry, *Proceedings of the National Academy of Sciences* **118**, e2100227118 (2021).
- [10] B. P. Bhowmik, H. G. E. Hentchel, and I. Procaccia, *Europhysics Letters* **137**, 46002 (2022).
- [11] K. Saitoh and B. P. Tighe, *Physical Review Letters* **122**, 188001 (2019).
- [12] B. P. Bhowmik and C. Ness, arXiv preprint arXiv:2308.08402 (2023).
- [13] J. Goyon, A. Colin, G. Ovarlez, A. Ajdari, and L. Bocquet, *Nature* **454**, 84 (2008).
- [14] K. Kamrin and G. Koval, *Physical Review Letters* **108**, 178301 (2012).
- [15] P. Chaudhuri and J. Horbach, *Physical Review E* **90**, 040301 (2014).
- [16] C. F. Schreck, R. S. Hoy, M. D. Shattuck, and C. S. O'Hern, *Physical Review E* **88**, 052205 (2013).
- [17] E. Tjhung and L. Berthier, *Physical Review Letters* **114**, 148301 (2015).
- [18] L. Galliano, M. E. Cates, and L. Berthier, *Physical Review Letters* **131**, 047101 (2023).
- [19] D. Hexner and D. Levine, *Physical Review Letters* **114**, 110602 (2015).
- [20] C. Ness and M. E. Cates, *Physical Review Letters* **124**, 088004 (2020).
- [21] A. Ghosh, J. Radhakrishnan, P. M. Chaikin, D. Levine, and S. Ghosh, *Physical Review Letters* **129**, 188002 (2022).
- [22] R. Mari, E. Bertin, and C. Nardini, *Physical Review E* **105**, L032602 (2022).
- [23] L. Milz and M. Schmiedeberg, *Physical Review E* **88**, 062308 (2013).
- [24] S. Lübeck, *International Journal of Modern Physics B* **18**, 3977 (2004).
- [25] G. I. Menon and S. Ramaswamy, *Physical Review E* **79**, 061108 (2009).
- [26] P. Pham, J. E. Butler, and B. Metzger, *Physical Review Fluids* **1**, 022201 (2016).
- [27] S. Oh, Y.-q. Song, D. I. Garagash, B. Lecampion, and J. Desroches, *Physical Review Letters* **114**, 088301 (2015).
- [28] R. E. Hampton, A. A. Mammoli, A. L. Graham, N. Tetlow, and S. A. Altobelli, *Journal of Rheology* **41**, 621 (1997).
- [29] J. J. Gillissen and C. Ness, *Physical Review Letters* **125**, 184503 (2020).
- [30] A. Vespignani and S. Zapperi, *Physical Review Letters* **78**, 4793 (1997).
- [31] A. Vespignani, R. Dickman, M. A. Muñoz, and S. Zapperi, *Physical Review Letters* **81**, 5676 (1998).
- [32] A. Hipke, S. Lübeck, and H. Hinrichsen, *Journal of Statistical Mechanics: Theory and Experiment* **2009**, P07021 (2009).
- [33] S.-L.-Y. Xu and J. M. Schwarz, *Physical Review E* **88**, 052130 (2013).
- [34] C. Cammarota and G. Biroli, *Proceedings of the National Academy of Sciences* **109**, 8850 (2012).
- [35] R. Das, B. P. Bhowmik, A. B. Puthirath, T. N. Narayanan, and S. Karmakar, *PNAS Nexus* **2**, pgad277 (2023).
- [36] B. P. Bhowmik, P. Chaudhuri, and S. Karmakar, *Physical Review Letters* **123**, 185501 (2019).
- [37] B. P. Bhowmik, S. Karmakar, I. Procaccia, and C. Rainone, *Physical Review E* **100**, 052110 (2019).